8-21-2012

Single crystal growth and superconductivity of Ca(Fe1-xCox)(2)As-2

Rongwei Hu
Iowa State University and Ames Laboratory

Sheng Ran
Iowa State University and Ames Laboratory

Warren E. Straszheim
Iowa State University and Ames Laboratory, wesaia@iastate.edu

Sergey L. Bud'ko
Iowa State University and Ames Laboratory, budko@ameslab.gov

Paul C. Canfield
Iowa State University and Ames Laboratory, canfield@ameslab.gov

Single crystal growth and superconductivity of Ca(Fe1-xCox)(2)As-2

Abstract

We report the single crystal growth of Ca(Fe1−x Co x)2As2 (0 ≤ x ≤ 0.082) from Sn flux. The temperature–composition phase diagram is mapped out based on the magnetic susceptibility and electrical transport measurements. The phase diagram of Ca(Fe1−x Co x)2As2 is qualitatively different from those of Sr and Ba; this could be due to both the charge doping and structural tuning effects associated with Co substitution.

Keywords

phase diagram, single crystal growth, superconductivity, magnetic properties, electrical properties

Disciplines

Condensed Matter Physics

Comments

This is an article published by Taylor & Francis as Hu, Rongwei, Sheng Ran, Warren E. Straszheim, Sergey L. Bud'ko, and Paul C. Canfield. "Single crystal growth and superconductivity of Ca (Fe1− x Co x) 2As2." *Philosophical Magazine* 92, no. 24 (2012): 3113-3120. DOI: 10.1080/14786435.2012.685774.

Philosophical Magazine

ISSN: 1478-6435 (Print) 1478-6443 (Online) Journal homepage: https://www.tandfonline.com/loi/tphm20

Single crystal growth and superconductivity of $Ca(Fe_{1-x}Co_x)_2As_2$

Rongwei Hu , Sheng Ran , Warren E. Straszheim , Sergey L. Bud'ko & Paul C. Canfield

To cite this article: Rongwei Hu , Sheng Ran , Warren E. Straszheim , Sergey L. Bud'ko & Paul C. Canfield (2012) Single crystal growth and superconductivity of $Ca(Fe_{1-x}Co_x)_2As_2$, Philosophical Magazine, 92:24, 3113-3120, DOI: 10.1080/14786435.2012.685774

To link to this article: https://doi.org/10.1080/14786435.2012.685774

Published online: 18 May 2012.

Philosophical Magazine
Vol. 92, No. 24, 21 August 2012, 3113–3120

Taylor & Francis
Taylor & Francis Group

Single crystal growth and superconductivity of $Ca(Fe_{1-x}Co_x)_2As_2$

Rongwei Hu*†, Sheng Ran, Warren E. Straszheim,
Sergey L. Bud'ko and Paul C. Canfield

Ames Laboratory, US DOE and Department of Physics and Astronomy, Iowa State University, Ames, IA 50011, USA

(*Received 2 March 2012; final version received 19 March 2012*)

We report the single crystal growth of $Ca(Fe_{1-x}Co_x)_2As_2$ ($0 \le x \le 0.082$) from Sn flux. The temperature–composition phase diagram is mapped out based on the magnetic susceptibility and electrical transport measurements. The phase diagram of $Ca(Fe_{1-x}Co_x)_2As_2$ is qualitatively different from those of Sr and Ba; this could be due to both the charge doping and structural tuning effects associated with Co substitution.

Keywords: phase diagram; single crystal growth; superconductivity; magnetic properties; electrical properties

$AEFe_2As_2$ (AE = Ca, Sr, Ba) of the 122 family are the most extensively studied materials among the various iron arsenic superconductors, since they possess the characteristic tetrahedrally coordinated square planar Fe sublattice, giving rise to lattice instability, antiferromagnetism (AFM) and superconductivity (SC) by chemical substitution, and are readily obtained in large single crystalline form [1–6]. $CaFe_2As_2$ is similar to the other two members; it undergoes a phase transition from a high temperature, tetragonal phase to a low temperature, orthorhombic/antiferromagnetic phase below 170 K [7]. Superconductivity can be induced in $CaFe_2As_2$ by substituting Fe with Co [8] or Rh [9] and As with P [10] and by application of non-hydrostatic pressure [11,12], as the tetragonal-orthorhombic/AFM transition is suppressed, strongly suggesting the connection between the AFM fluctuations and SC. However, the physical properties of the single crystals of $CaFe_2As_2$ are remarkably dependent on the crystal growth procedure. It has been shown that crystals quenched from high temperature using FeAs flux exhibit a transition from a high temperature, tetragonal to a low temperature, non-magnetic, collapsed tetragonal phase below 100 K in contrast to the behavior of $CaFe_2As_2$ grown from Sn flux [13]. For Co doping, the as-grown, single crystals grown from FeAs-CoAs self-flux, decanted at 1000°C, do not show any SC as opposed to the

*Corresponding author. Email: rwhu@umd.edu
†Present address: Center for Nanophysics & Advanced Materials and Department of Physics, University of Maryland, College Park MD 20742-4111, USA.

ISSN 1478–6435 print/ISSN 1478–6443 online

http://dx.doi.org/10.1080/14786435.2012.685774
http://www.tandfonline.com

corresponding ones grown from Sn flux [14]. Moreover, there is a competing phase of $CaFe_4As_3$ growing concomitantly with $CaFe_2As_2$ from Sn flux [7]. Therefore details in the crystal growth and effects of Co doping in $CaFe_2As_2$ need to be clarified. In this work, we performed a study of the single crystal growth of $Ca(Fe_{1-x}Co_x)_2As_2$ out of Sn flux and showed the dependence of the magnetic susceptibility and resistivity on Co doping.

Single crystals of $Ca(Fe_{1-x}Co_x)_2As_2$ were grown from Sn flux in two steps. In order to obtain homogeneous Co substitution for Fe, polycrystalline $Ca(Fe_{1-x}Co_x)_2As_2$ were prepared first by heating stoichiometric mixtures of Ca, FeAs and CoAs at 900°C for 24 hours. The polycrystalline sample was ground and pelletized for a second time sintering at 900°C. Then polycrystalline $Ca(Fe_{1-x}Co_x)_2As_2$ and Sn with a ratio of 1:30 were placed in an alumina crucible and sealed in amorphous silica tubes. The sealed ampoule was heated to 1100°C and slowly cooled to 600°C after which the Sn flux was decanted [15]. This procedure is similar to that in Ref. [16]. Early work on crystal growth of $CaFe_2As_2$ using Sn flux has identified a needle-shaped orthorhombic phase, $CaFe_4As_3$, growing together with $CaFe_2As_2$ out of Sn flux [7]. Our crystal growth using the similar procedure as in [16] showed that there was a significant amount of $CaFe_4As_3$ phase by following the above procedure. For Co doping, the formation of the competing phase may change the composition of the liquid solution, thus it causes complex dependence of the doping concentration of the resulted single crystals on growth conditions. An excess of Ca was added to the polycrystalline and Sn mixture and an optimal $Ca_{1.5}(Fe_{1-x}Co_x)_2As_2$ was found to be effective for eliminating the $CaFe_4As_3$ phase. Moreover, there is a solubility problem of $Ca(Fe_{1-x}Co_x)_2As_2$ in Sn. For the ratio of 1:30, in addition to $Ca(Fe_{1-x}Co_x)_2As_2$ single crystals, there was some undissolved polycrystalline powder after decanting. By changing the ratio to 1:45, we were able to completely dissolve the starting polycrystal. Therefore in our work, in order to eliminate the competing phase $CaFe_4As_3$, an optimal starting stoichiometry has been found, i.e. $Ca_{1.5}(Fe_{1-x}Co_x)_2As_2 : Sn = 1{:}45$. The as-grown single crystals were thin plate-like with typical dimension $4 \times 4 \times 0.2\,mm^3$.

Crystals were characterized by powder X-ray diffraction using a Rigaku Miniflex X-ray diffractometer. The actual chemical composition was determined using wavelength dispersive X-ray spectroscopy (WDS) in a JEOL JXA-8200 electron microscope, by averaging ten spots on the crystal surface. Magnetic susceptibility was measured in a Quantum Design MPMS, SQUID magnetometer. In-plane AC resistivity ρ_{ab} was measured by a standard four-probe configuration within MPMS using an LR-700 resistance bridge (frequency = 16 Hz, current = 1–3 mA).

Figure 1a shows the actual concentration of Co, x_{WDS}, as a function of the nominal $x_{nominal}$, of two series of crystals: using stoichiometric, nominal composition, polycrystalline feedstock, and using polycrystalline feedstock that had 50% excess Ca. The compositional spread of the ten measured spots is taken as the error bar. In contrast to the results in [16], x_{WDS} deviates from linear dependence on $x_{nominal}$. After the elimination of the competing $CaFe_4As_3$ phase with 50% excess Ca, x_{WDS} generally increases and has a larger compositional spread, but the curve follows the same trend as the stoichiometric one and the significant non-monotonicity is still present. It is noteworthy that for $x_{nominal}$ greater than 0.10, the corresponding x_{WDS} decreases dramatically. This behavior suggests difficulties

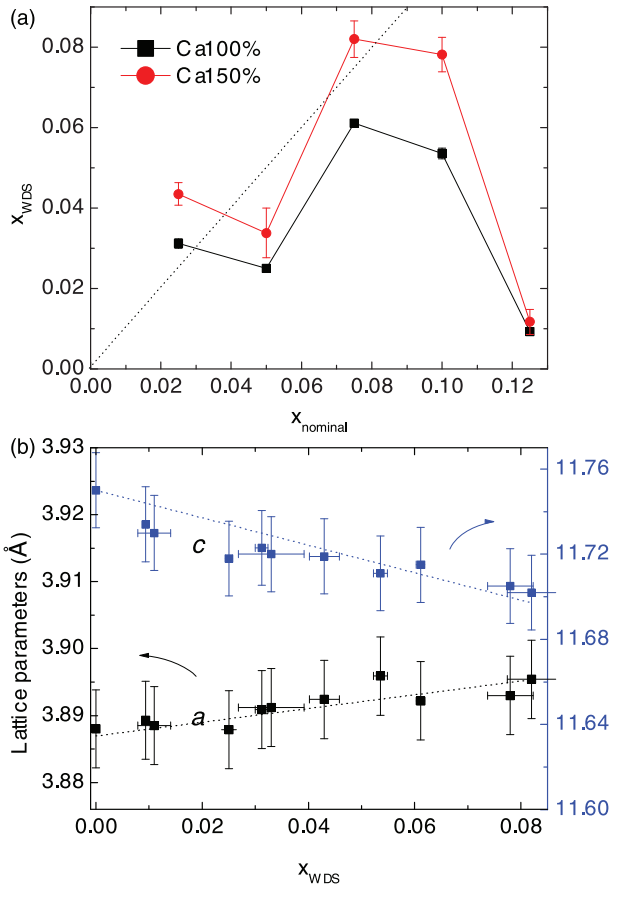

Figure 1. (a) Actual Co concentration as a function of nominal concentration. Black squares represent the series with stoichiometric starting composition; red circles represent the series with 50% excess Ca in starting composition. The dotted line indicates the ideal slope equal to 1. (b) Lattice parameters vs. Co doping. Lines are guides to the eye.

associated with solubility and once again highlights the need to perform WDS measurements on the grown samples. The nonlinear dependence of the actual concentration could be related to a different synthesis approach from [16]. The solubility limit, which is determined to be $x = 0.082$, may also give rise to this complex dependence of x_{WDS}. When the lattice parameters (from both series) are plotted as a function of x_{WDS} (Figure 1b), there is a clear linear dependence of a and c parameters on Co-substitution level. The lattice parameters refined by Rietica are shown in Figure 1b. Lattice parameter a increases by 0.1% whereas c decreases by 0.4% for $x_{WDS} = 0.082$, similar to the trend in $Sr(Fe_{1-x}Co_x)_2As_2$. This is also in agreement with the results of [16], where c linearly decreases, at $x_{EDX} = 0.09$ $\Delta c/c = 0.5\%$, although we do not obtain samples with Co doping higher than 0.08. There are two pairs of concentrations very close to each other by coincidence, i.e. $x_{WDS} = 0.009$, 0.011 and 0.031, 0.033. Only $x_{WDS} = 0.009$ and 0.031 samples were characterized in the following study.

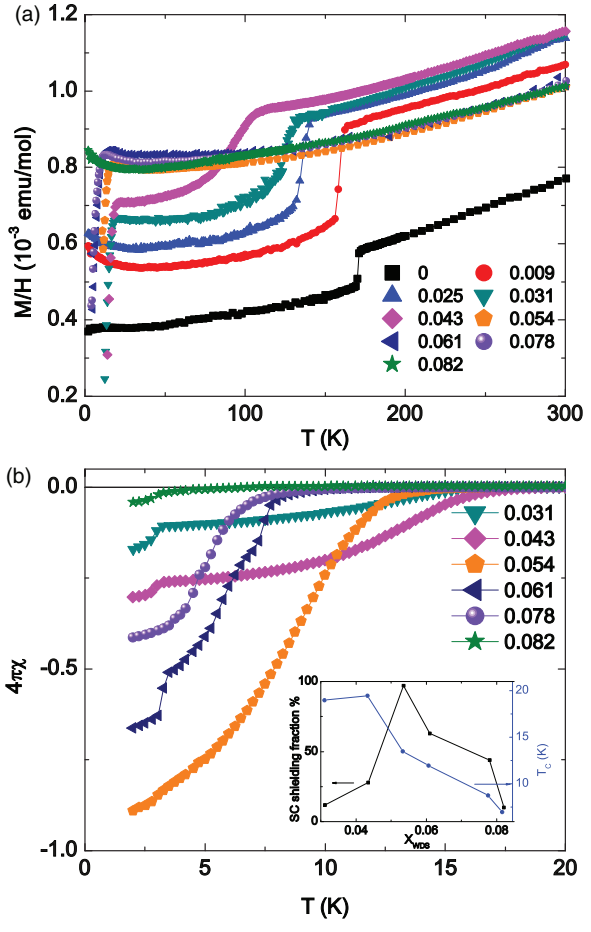

Figure 2. (a) In-plane magnetic susceptibility measured in a magnetic field of 10 kOe as a function of temperature. (b) Zero-field-cooled magnetic susceptibility in 50 Oe. The inset shows the variation of superconducting shielding fraction and T_c.

In-plane magnetic susceptibility of $Ca(Fe_{1-x}Co_x)_2As_2$ is shown in Figure 2a for a magnetic field of 10 kOe. The structural/magnetic transition of the parent $CaFe_2As_2$ at 170 K is suppressed progressively by Co doping consistent with [16], until it is completely suppressed at $x = 0.054$. Superconductivity is first detected for $x = 0.031$ and the superconducting transition temperature, T_c, decreases with further substitution. Figure 2b shows the zero-field-cooled (ZFC) magnetic susceptibility curves in an applied field of 100 Oe. The small dip at 3.5 K for some curves is due to small Sn flux droplets on the crystal surface. The superconducting shielding fraction, with the contribution from Sn subtracted, varies with doping levels. The highest T_c occurs at $x = 0.043$ whereas the largest volume fraction is reached at $x = 0.054$ with slightly lower T_c (Figure 2b inset). This is similar to what is observed in [16].

Electrical resistance data, normalized to their room temperature values, are shown in Figure 3a for the Sn flux grown crystals. The small drop of resistivity for the undoped $CaFe_2As_2$ below 10 K is widely observed in our single crystals as well as

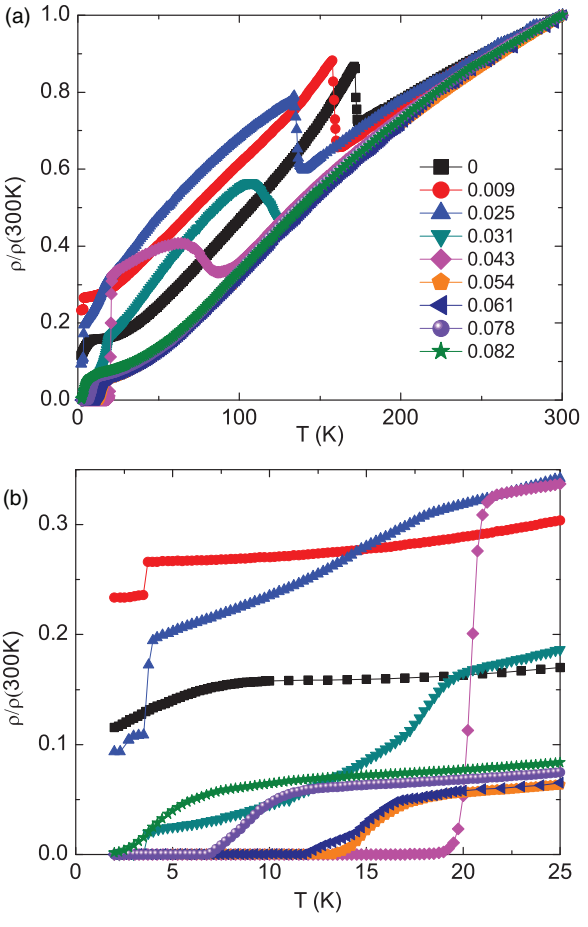

Figure 3. (a) Temperature dependence of the normalized resistivity of $Ca(Fe_{1-x}Co_x)_2As_2$. (b) Expanded view of normalized resistivity at low temperatures.

in the work of others [7,16], and is likely related to stress/strain induced superconductivity. It has been demonstrated that superconductivity can be induced and how sensitive the $CaFe_2As_2$ is to non-hydrostatic pressure [11,12]. Therefore small deformation or stress in the crystal may give rise to a partial volume superconducting phase. The anomaly at 170 K for the pure $CaFe_2As_2$ is suppressed with Co doping, remains sharp until $x_{WDS} = 0.025$ and becomes broad for $x_{WDS} = 0.031$ and 0.043. (It should be noted that this broadening coincides with the sudden onset of superconductivity.) Figure 3b shows the low temperature normalized resistance. The small jump at 3.5 K is due to remanent Sn flux on the crystal. Although $x_{WDS} = 0.031$ shows partial magnetic shielding and its resistance starts to drop at about the same onset temperature, zero resistance is not reached. A complete superconducting transition is observed for $x_{WDS} \geq 0.043$ and T_c gradually decreases with doping in good agreement with the magnetic susceptibility measurements. Nanoscale inhomogeneity and strain due to Co doping may result in wide transitions. But considering the variation and small number of the

superconducting volume fraction, SC may not be bulk for many of the $Ca(Fe_{1-x}Co_x)_2As_2$ samples. Other experimental techniques, e.g. magneto-optical imaging, specific heat, or STM spectroscopy will be required to further clarify the nature/homogeneity of the low temperature state.

Based on the magnetic and transport measurements, the T-x_{WDS} phase diagram for $Ca(Fe_{1-x}Co_x)_2As_2$ is mapped out in Figure 4a. The structural and magnetic transitions are inferred from $d\chi/dT$ and $d(\rho/\rho_{300\,K})/dT$ using the same criteria in [16]. The superconducting transition temperature T_c is inferred from the first deviation from the normal magnetic susceptibility of the ZFC curve. Resistive onset and offset of T_c values are inferred from the intercepts of the steepest slope with the normal state and zero resistance respectively. The simultaneous structural and magnetic transition of the pure $CaFe_2As_2$ is monotonically suppressed by Co doping, but as

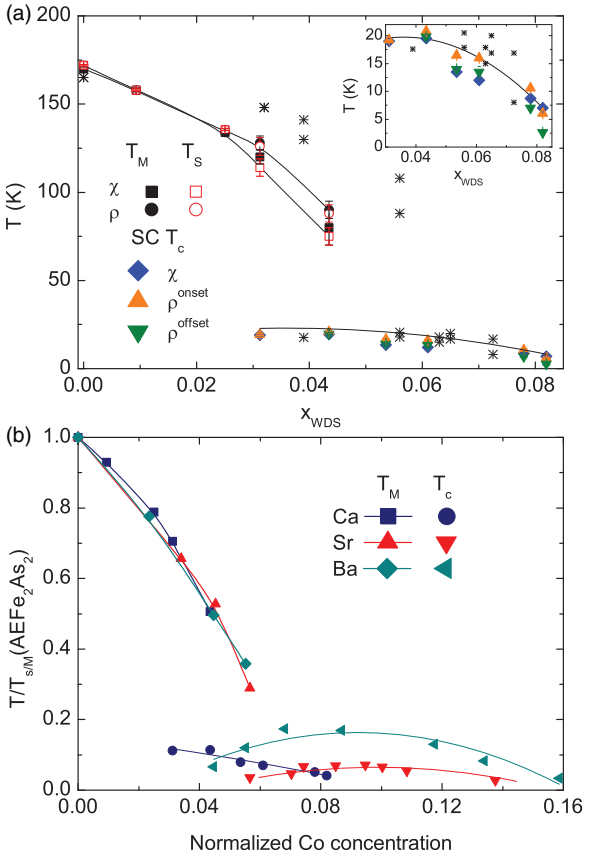

Figure 4. (a) T-x phase diagram of $Ca(Fe_{1-x}Co_x)_2As_2$. Solid lines are guides to the eye. The inset shows the superconducting region. Black asterisks are the data from [16] inferred from resistance. (b) Comparison of the Ca (this work), Sr [17], and Ba [4] phase diagrams of Co doping. T_cs are inferred from magnetic susceptibility measurements. Normalization: T-axis is normalized by the $T_{S/M}$ of the respective parent compound; (Sr) x-axis multiplied by 0.81; (Ba) x-axis multiplied by 1.18.

seen from χ and ρ, the transition remains sharp for low dopings $x_{WDS} \leq 0.025$, and no discernible splitting of both transitions can be observed. For $x_{WDS} = 0.031$ and 0.043, the transition broadens and it is possible to infer an upper structural transition and a lower magnetic transition, similar to $Ba(Fe_{1-x}Co_x)_2As_2$ [4]. To compare the reported phase diagram of $Ca(Fe_{1-x}Co_x)_2As_2$ in [16] with ours, we plot the data points (black asterisks) inferred from resistance measurements of [16] in Figure 4a. As can be seen, though our phase diagram shows a faster suppression of the magnetic and structural transitions by Co doping, SC occurs roughly with the same T_c in similar region. It should be noted that the actual Co concentration reaches up to 0.15 in [16], but only the onset of resistive or no superconducting transition is observed above $x = 0.09$, consistent with our observations. We might imagine that an overestimate (underestimate) of the Co concentration in [16] (our work) will shift the phase diagram.

Different from the superconducting dome in $Sr(Fe_{1-x}Co_x)_2As_2$ [17] and $Ba(Fe_{1-x}Co_x)_2As_2$ [4], the onset of SC in $Ca(Fe_{1-x}Co_x)_2As_2$ appears abruptly at high temperature and gradually decreases with Co substitution. In order to compare all three cases of Co doping, the magnetic transition boundaries of Sr and Ba are collapsed on to that of Ca, namely the transition temperatures are normalized by that of the pure parent $AEFe_2As_2$ and the Co concentrations of Sr and Ba are scaled so as to get to a single manifold in Figure 4b. Whereas both the Ba and Sr series manifest a maximum T_c value close to the Co substitution level that drives the magnetic/structural phase transitions to zero, the Ca series manifests maximum T_c values deep in the ordered region and has SC disappearing near the substitution levels needed to suppress the antiferromagnetic/structural phase transition. For the Co substituted Ca122 series the sudden onset of SC may instead be correlated with the splitting of the structural/magnetic phase transition that takes place for $0.025 < x < 0.031$. The reason for this difference is currently not well understood, but may be related to the extreme pressure and strain sensitivity of $CaFe_2As_2$ as a host material. Unlike Co substituted $BaFe_2As_2$ or $SrFe_2As_2$, it is possible that the changes in lattice parameter seen in Co substituted $CaFe_2As_2$ play a more important role in determining the phase diagram and represent an additional term to the changes in band filling associated with Co substitution.

In summary, $Ca(Fe_{1-x}Co_x)_2As_2$ ($0 \leq x \leq 0.082$) have been grown out of Sn flux. We report the details of single crystal growth and their magnetic susceptibility and electrical transport properties. The properties of single crystals are dependent on the growth procedure. The phase diagram of $Ca(Fe_{1-x}Co_x)_2As_2$ shows a half-dome-like superconducting region, different from those of $Sr(Fe_{1-x}Co_x)_2As_2$ and $Ba(Fe_{1-x}Co_x)_2As_2$. The electron doping as well as the chemical pressure probably are both responsible for determining the phase boundary

Acknowledgments

This work was carried out at the Iowa State University and supported by the AFOSR-MURI grant #FA9550-09-1-0603 (R.H. and P.C.C.). Part of this work was performed at Ames Laboratory, US DOE, under contract #DE-AC02-07CH 11358 (S.R., S.L.B. and P.C.C.). S.L. Bud'ko also acknowledges partial support from the State of Iowa through Iowa State University.

References

[1] M. Rotter, M. Tegel and D. Johrendt, Phys. Rev. Lett. 101 (2008) p.107006.
[2] P.C. Canfield and S.L. Bud'ko, Ann. Rev. Condensed Matter Phys. 1 (2010) p.27.
[3] K. Sasmal, B. Lv, B. Lorenz, A. Guloy, F. Chen, Y. Xue and C.W. Chu, Phys. Rev. Lett. 101 (2008) p.107007.
[4] N. Ni, A. Thaler, J.Q. Yan, A. Kracher, E. Colombier, S.L. Bud'ko and P.C. Canfield, Phys. Rev. B 82 (2010) p.024519.
[5] D. Kasinathan, A. Ormeci, K. Koch, U. Burkhardt, W. Schnelle, A. Leithe-Jasper and H. Rosner, New J. Phys. 11 (2009) p.025023.
[6] Y. Izyumov and E. Kurmaev, Springer Mater. Sci. 143 (2010) p.57.
[7] N. Ni, S. Nandi, A. Kreyssig, A.I. Goldman, E.D. Mun, S.L. Bud'ko and P.C. Canfield, Phys. Rev. B 78 (2008) p.014523.
[8] N. Kumar, R. Nagalakshmi, R. Kulkarni, P.L. Paulose, A.K. Nigam, S.K. Dhar and A. Thamizhavel, Phys. Rev. B 79 (2009) p.012504.
[9] Y. Qi, L. Wang, Z. Gao, D. Wang, X. Zhang, C. Wang, C. Yao and Y. Ma, New J. Phys. 13 (2011) p.033020.
[10] S. Kasahara, T. Shibauchi, K. Hashimoto, Y. Nakai, H. Ikeda, T. Terashima and Y. Matsuda, Phys. Rev. B 83 (2011) p.060505(R).
[11] P.C. Canfield, S.L. Bud'ko, N. Ni, A. Kreyssig, A.I. Goldman, R.J. McQueeney, M.S. Torikachvili, D.N. Argyriou, G. Luke and W. Yu, Physica C 469 (2009) p.404.
[12] M.S. Torikachvili, S.L. Bud'ko, N. Ni, P.C. and Canfield and S.T. Hannahs, Phys. Rev. B 80 (2009) p.014521.
[13] S. Ran, S.L. Bud'ko, D.K. Pratt, A. Kreyssig, M.G. Kim, M.J. Kramer, D.H. Ryan, W.N. Rowan-Weetaluktuk, Y. Furukawa, B. Roy, A.I. Goldman and P.C. Canfield, Phys. Rev. B 83 (2011) p.144517.
[14] S. Ran, private communication.
[15] P.C. Canfield and Z. Fisk, Phil. Mag. B 65 (1992) p.1117.
[16] L. Harnagea, S. Singh, G. Friemel, N. Leps, D. Bombor, M. Abdel-Hafiez, A.U.B. Wolter, C. Hess, R. Klingeler, G. Behr, S. Wurmehl and B. Buchner, Phys. Rev. B 83 (2011) p.094523.
[17] R. Hu, S.L. Bud'ko, W.E. Straszheim and P.C. Canfield, Phys. Rev. B 83 (2011) p.094520.